PUBLICATION VI

Microelectromechanical delay lines with slow signal propagation

In: Journal of Micromechanics and Microengineering 2006. Vol. 16, pp. 1854–1860.
Reprinted with permission from the publisher.

www.iop.org/journals/jmm

Microelectromechanical delay lines with slow signal propagation

Ari T Alastalo, Jyrki Kiihamäki and Heikki Seppä

VTT Technical Research Centre of Finland, P.O.B. 1000, FI-02044 VTT, Finland

E-mail: `ari.alastalo@vtt.fi`

Abstract. A slow-wave microelectromechanical delay line, composed of a chain of coupled resonators, is introduced. The delay line has a bandpass response and, depending on structural details, signal group velocity can be as low as $\sim$ 10 m/s that is over 100 times smaller than for acoustical SAW or BAW delay lines. Properties of the delay line are analyzed theoretically and the theory is verified in measurements.

PACS numbers: 84.40.Az, 85.85.+j

1. Introduction

Acoustic wave propagation in solids has for a long time been utilized in electronics to implement various components such as resonators, filters, and delay lines. In these applications, one benefits from i) low attenuation of acoustic waves in crystalline materials and ii) low acoustic wave velocity compared to electromagnetic waves. Low attenuation enables high Q values of mechanical resonators such as in quartz-based oscillators that are widely utilized as low-phase-noise frequency standards in mobile communication devices. Low-loss propagation is also essential in surface-acoustic-wave (SAW) and bulk-acoustic-wave (BAW) filters [1]. The acoustic SAW and BAW velocities are of the order of 5000 m/s that is approximately 10^5 times smaller than the wave velocities for electromagnetic transmission lines. Thus large signal delays can be produced with small-sized components. SAW and BAW delay lines and filters can be used up to several GHz frequencies. The microelectromechanical delay line, presented in this paper, enables a further reduction of group velocity by a factor of $\sim$ 100 for signal frequencies in the HF range (3-30 MHz) and below, which are relevant frequencies, for example, for wireless communication of low-datarate sensor applications and RFID.

Acoustic delays have been utilized in several applications. For example, in wireless passive SAW RFID tags and sensors, the transmitted data is coded into a multitude of reflections of a SAW pulse that is generated (in response to a received radio pulse) and detected by an antenna connected to a SAW chip [2, 3]. In these applications, long acoustic delays and short transmission distances guard against interference from multipath radio propagation. In radar systems, delay lines are used, for example, to create a delayed replica of the transmit signal to correlate with the received signal reflected from the target [4], to compensate for phase errors in FMCW radars [5] or to simulate a target [6]. In delay-line oscillators, long delay stabilizes the frequency and suppresses off-carrier phase noise [7, 8, 9, 10]. Delay-line based information processing has been applied to implement convolution, time inversion and Fourier transforms [11, 12, 13]. Analog delays are also proposed for novel ultra-wideband receivers [14]. In video systems, delay lines are used, for example, in event recorders and action replay.

The recent advances in microelectromechanical systems (MEMS) technology have opened the possibility for creating minituriased acoustical devices. As an example, a micromechanical resonator based on BAW-operation has been demonstrated to be well suited for a high-spectral-purity oscillator [15] in mobile-communication applications. Integrability of MEMS technology with CMOS electronics as well as size reduction and power savings of MEMS components compared to off-chip solutions (such as SAW devices) facilitate design of efficient single-chip radio transceivers that could revolutionise wireless communication devices [16].

In this paper, a narrow-band capacitively-coupled dispersive MEMS delay line for signals at HF frequencies is analyzed in detail. The delay line consists of a chain of coupled and anchored micromechanical resonators and can have a 100 times smaller signal group velocity than in SAW or BAW delay lines thus facilitating miniaturization of delay-line components. A similar structure for lower frequencies was introduced in [17]. In this paper, general theory of anchored spring-mass-chain delay lines is formulated and an electrical-equivalent model is derived. The theory is verified with measurements of two different fabricated delay lines composed of 80 tuning-fork resonators in series. Design improvements necessary for practical applications are discussed.

2. Theory

The anchored spring-mass-chain waveguide, shown in figure 1 without dissipation, is composed of elementary resonators that can be modelled with two moving masses, m, that are coupled with a spring k and anchored to a stationary support with springs k'. Except for the ends, the chain is periodic with period a. The waveguide can be seen as a high-order bandpass filter [16, 18] with identical stages. Transduction between electrical signals and a mechanical wave propagating along the chain is done with capacitive parallel-plate transducers with gap d, area BH and rest capacitance $C_0 = \epsilon_0 BH/d$. Here H is the thickness of the device (perpendicular to the plane of the picture) and B is the length of the transducers as shown in figure 1. The model in figure 1(e) is also applicable, for example, for periodic resonator chains where the inter-stage coupling is done with a capacitor instead of the mechanical spring. In this paper, damping is not considered in theory but is modelled in simulations. For low losses, this results in good theoretical estimates of the properties of the waveguide.

The elementary resonator of figure 1 has two fundamental modes of vibration with

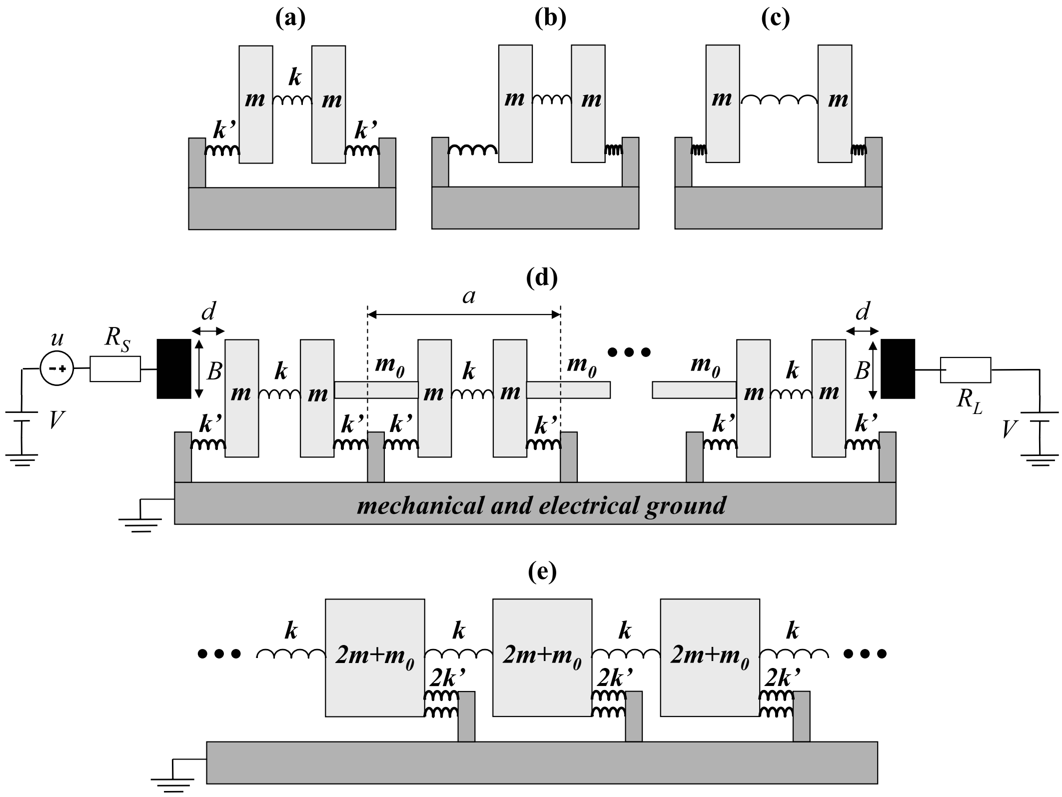

Figure 1. (a) Rest position of an elementary two-mode resonator with symmetric (b) and antisymmetric (c) eigenmodes. (d) Delay line consisting of capacitive input (left) and output (right) transducers with gap d and a chain of coupled resonators. Except for the ends of the chain, the waveguide can be modelled as shown in (e). Losses are not indicated.

resonance frequencies

$$\omega_s = \sqrt{\frac{k'}{m}} \tag{1}$$

$$\omega_a = \sqrt{\frac{2k + k'}{m}}. \tag{2}$$

In the symmetric mode, with resonance frequency ω_s (1), the masses move in phase while in the antisymmetric mode, with frequency ω_a (2), there is a 180° phase difference between the mass motions. A useful parameter is the ratio of the anchoring spring k' to the coupling spring k, determined by ω_a/ω_s as

$$K \equiv k'/k = \frac{2}{(\omega_a/\omega_s)^2 - 1}. \tag{3}$$

For a particular resonator geometry, the ratio of the resonance frequencies is obtained, for example, in FEM eigenmode analysis or in measurements.

A periodic chain of coupled resonators can vibrate and carry signals at frequencies allowed by the dispersion relation $\omega(\kappa)$ that gives the frequency ω as a function of the wave vector $\kappa \equiv 2\pi/\lambda$, where λ is the wavelength. For the anchored chain of figure 1,

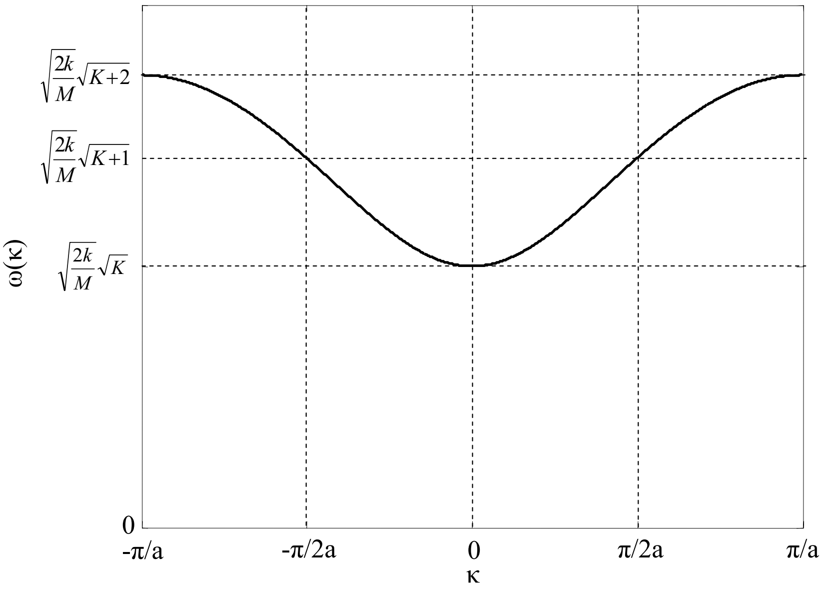

Figure 2. Dispersion relation for the anchored spring-mass chain of figure 1.

the dispersion relation is found as a generalization of the familiar text-book result for periodic unanchored (free) chains [19]. One obtains for the anchored chain

$$\omega(\kappa) = \sqrt{\frac{2k}{M}}\sqrt{1-\cos(\kappa a)+K}, \tag{4}$$

where $M \equiv 2m + m_0$ is the total coupled-resonator mass, a is the period of the chain and the wave vector $\kappa \in [-\pi/a, \pi/a]$ is restricted to the first Brillouin zone [19]. The dispersion relation (4) is illustrated in figure 2. As opposed to the low-pass character of free chains, nonzero k' forbids zero-frequency oscillations and results in passband response.

Group velocity for signal propagation along the chain is found from (4) as

$$v_g = \frac{\partial\omega}{\partial\kappa} = \frac{a}{2}\sqrt{\frac{2k}{M}}\frac{\sin(\kappa a)}{\sqrt{1-\cos(\kappa a)+K}}, \tag{5}$$

and is seen to differ from the phase velocity $v_{ph} = \omega/\kappa$. For the center frequency $\omega_0 = 2\pi f_0$ and bandwidth $\Delta\omega = 2\pi\Delta f$ of the line one finds

$$\omega_0 = \omega(\frac{\pi}{2a}) = \sqrt{\frac{2k}{M}}\sqrt{K+1} \tag{6}$$

$$\Delta\omega = \omega(\frac{\pi}{a}) - \omega(0) = \sqrt{\frac{2k}{M}}\left(\sqrt{K+2} - \sqrt{K}\right). \tag{7}$$

At the center of the passband, one obtains for the phase and group velocities

$$v_{ph}^0 \equiv \frac{\omega}{\kappa}\Big|_{\omega_0} = \frac{2a}{\pi}\sqrt{\frac{2k}{M}}\sqrt{K+1} \tag{8}$$

$$v_g^0 \equiv \frac{\partial\omega}{\partial\kappa}\Big|_{\omega_0} = \frac{a}{2}\sqrt{\frac{2k}{M}}\frac{1}{\sqrt{K+1}} \tag{9}$$

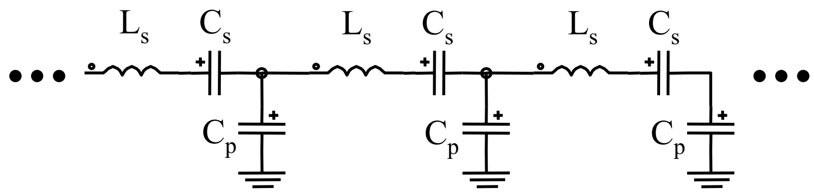

Figure 3. Electrical-equivalent model for the spring-mass-chain transmission line in figure 1 for center-band operation.

illustrating, again, clearly the dispersive character of the spring-mass chain.

For single capacitively-coupled MEMS resonators with spring constant k, mass m and quality factor Q, the electrical equivalent is a series RLC circuit (see, for example, [20]) with $R = \sqrt{km}/(Q\eta^2)$, $L = m/\eta^2$ and $C = \eta^2/k$, where $\eta = C_0V/d$ is the electromechanical coupling coefficient while C_0 is the transducer rest capacitance, V the bias voltage and d the transducer gap as in figure 1. To find a similar representation for the spring-mass-chain transmission line, the propagation constant κa in (4) is solved and its square, $(\kappa a)^2 = Z_sY_p$, [21] is expanded as a power series with respect to ω^2 around the passband center. Here Z_s is the series impedance and Y_p is the shunt admittance of the waveguide per unit length. One finds

$$(\kappa a)^2 = \left\{ \frac{j\omega M}{\eta^2} + \frac{2k}{j\omega\pi\eta^2} \left[\pi(1+K) - \left(\frac{\pi}{2}\right)^2 \right] \right\} \frac{j\omega\pi\eta^2}{2k}, \tag{10}$$

where $Z_s = j\omega L_s + 1/(j\omega C_s)$ and $Y_p = j\omega C_p$ can now be identified, as shown in figure 3, with

$$L_s = \frac{M}{\eta^2} \tag{11}$$

$$C_s = \frac{\pi\eta^2}{2k\left[\pi(1+K) - (\pi/2)^2\right]} \tag{12}$$

$$C_p = \frac{\pi\eta^2}{2k}. \tag{13}$$

Consequently, one obtains the characteristic impedance of the line as [21]

$$Z_c = \sqrt{\frac{Z_s}{Y_p}} = \frac{\sqrt{kM}}{\eta^2\sqrt{2(K+1)}}. \tag{14}$$

The scaling of the terms in (10) with the squared coupling coefficient, η^2, is done in order to have the correct $Z_c \sim 1/\eta^2$ dependence of the characteristic impedance as verified in simulations.

It is seen that increasing the strength of the anchoring spring k' with respect to the coupling spring k increases the center frequency (6) and phase velocity (8) while decreasing bandwidth (7), group velocity (9) and the characteristic impedance (14) that, typically, is much higher than 50 Ω with electrostatic coupling. Furthermore, for higher K, the variation of the group velocity as a function of frequency at band center

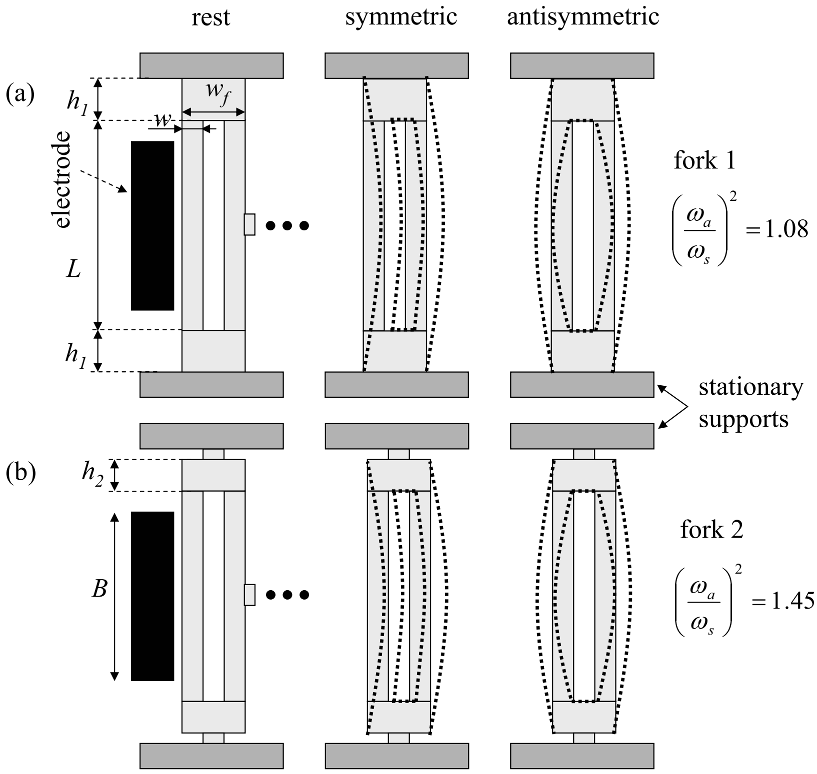

Figure 4. Two different tuning-fork designs (fork 1 in (a) and fork 2 in (b)) for the elementary resonator of figure 1.

is reduced. For good signal coupling and long delays, it is thus desirable to have K as high as possible.

3. Design with tuning-fork resonators

One possible realization for the elementary resonators in figure 1 is the doubly-supported tuning-fork structure for which two geometries are schematically shown in figure 4. For both designs, the distance between the anchoring connects to the stationary supports is the same and the vibrating beams are of same size (5 μm $\times$50 μm). The only difference in the designs is at the anchoring structure. Fork 2 (figure 4(b)) has a weaker coupling to the support than fork 1 and, correspondingly, a stronger coupling between the beams (stronger k and smaller K) resulting in wider frequency separation between the eigenmodes and higher characteristic impedance. The dimensions and central properties of the tuning forks as well as corresponding transmission lines composed of 80 resonators are collected in table 1. The FEM results are calculated with ANSYS® .

Table 1. Design values and FEM results for the parameters of the tuning-fork resonators of figure 4. For Z_c a bias voltage of $V = 25.6$ V has been used. For the group delay T_g^0, a chain of 80 resonators, with a total length of the line of $L_{line} = 1.4$ mm, is considered.

	fork 1	fork2	unit	comment
h	$h_1 = 10$	$h_2 = 7.5$	μm	design
f_s	13.573	11.406	MHz	FEM
f_a	13.992	13.748	MHz	FEM
k'	17.3	12.4	kN/m	FEM
K	31.9	4.42		FEM
M	4.77	4.81	ng	(1), (2)
f_0	13.8	12.6	MHz	(6)
Δf	0.42	2.34	MHz	(7)
v_{ph}^0	965	884	m/s	(8)
v_g^0	23	128	m/s	(9)
T_g^0	60.8	10.9	μs	$\frac{L_{line}}{v_g^0}$
Z_c	0.96	5.42	MΩ	(14)
L	50		μm	design
B	45		μm	design
w	5		μm	design
w_f	15		μm	design
d	200		nm	design
H	10		μm	design
a	17.5		μm	design
L_{line}	1.4		mm	design
C_0	20		fF	

4. Experimental verification

To verify the spring-mass-chain model, periodic narrow-gap single-crystal-silicon resonator chains, corresponding to the tuning-fork designs in figure 4 and table 1, were fabricated on silicon-on-insulator (SOI) wafers and characterized. Figure 5 shows a SEM picture of the fabricated resonator chains. The number of coupled resonators in the chain is 80 as considered in table 1. One thus expects center-band group delays of

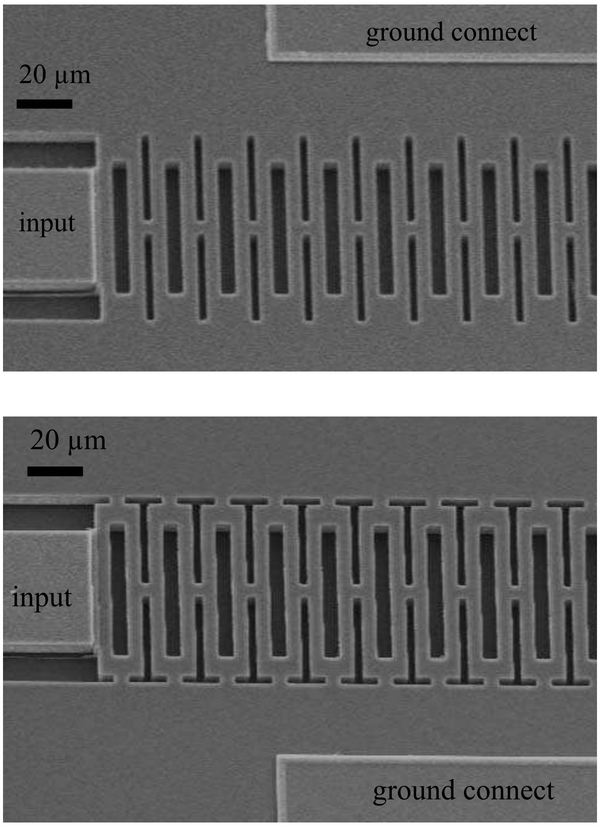

Figure 5. SEM picture of tuning-fork chains composed of fork 1 (up) and fork 2 (lower) of table 1.

45 μs and 10 μs for 1.4 mm long tansmission lines made of fork 1 and fork 2 of figure 4, respectively. As the fabrication process is detailed elsewhere [22], only the experimental set-up and results are given here.

Figure 6 shows a schematic of the measurement and simulation setup. The mechanical transmission lines, chain 1 and chain 2 of figure 5, and their input and output transducers are represented by the black-box components. Component values of figure 6 are collected in table 2.

In measurements, the input (in) and output (out) are connected to an HP 4195A network analyzer. The resonator chains, biasing circuits and the differential low-noise preamplifier (AD8129) are kept in a vacuum chamber with a pressure of 3 μbar. Only one of the transmission lines is measured at a time with nonzero bias voltage. In the other branch, with zero bias, signal propagates only through the parasitic feed-through capacitance C_{thr1} or C_{thr2}. Consequently, the differential readout suppresses the feed-through signals and amplifies only the signal propagating through the mechanical waveguide. As C_{thr1} and C_{thr2} are slightly different, trimmer capacitors, C_{tune1} and C_{tune2}, are utilized in the waveguide inputs such that a common-mode-rejection ratio (CMRR) of 61 dB is achieved. Here the feed-through capacitances of the two devices are almost equal and thus the cancellation is conveniently done using the unbiased

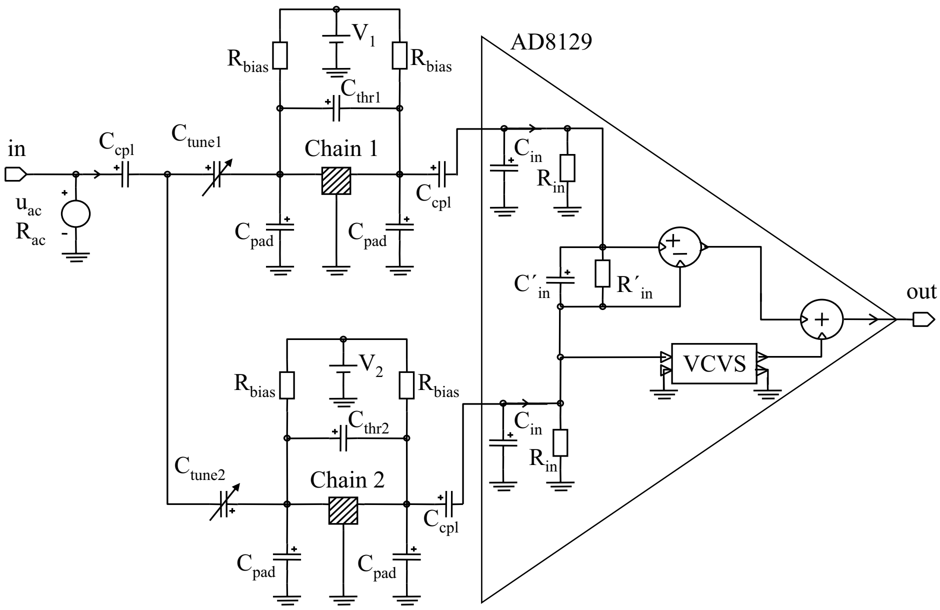

Figure 6. Measurement and simulation setup.

Table 2. Parameter values for the measurement and simulation setup of figure 6.

parameter	value	unit
C_{thr1}	≈ 30	fF
C_{thr2}	≈ 30	fF
C_{tune1}	$\in [0.5, 15]$	pF
C_{tune2}	$\in [0.5, 15]$	pF
C_{cpl}	100	nF
C_{pad}	360	fF
C_{in}	4	pF
C'_{in}	3	pF
R_{ac}	50	Ω
R_{bias}	3.6	MΩ
R_{in}	4	MΩ
R'_{in}	1	MΩ

component as a reference. More generally, one can use a tuneable capacitance of the same order as the feed-through capacitances for the reference. In addition to the high CMRR, the preamplifier has a differential gain of 17 dB. The transmission S_{21} is measured with respect to a short connecting the input and output of the network analyzer.

In simulations, the electrical circuit, transducers and the mechanical resonator chains are modelled in Aplac® [23] circuit simulator. The preamplifier is modelled as shown in figure 6. The voltage-controlled voltage source (VCVS) is used to tune the common-mode-rejection ratio to the measured level of 61 dB.

Figure 7 shows the measured and simulated responses for the two different spring-mass-chain transmission lines. The simulation results that reasonably well fit the measurements are obtained by varying the electrode length B, mechanical quality factor Q of the elementary resonators, the ratio of the spring coefficients K, the anchoring spring k' and the transducer gap d from the design values given in table 1. The fitting values for these parameters are given in table 3. The difference between the designed (table 1) and fitted (table 3) values for the spring coefficients can be explained by i) a finite stiffness of the support (assumed stationary in design as indicated in figure 4) at the anchoring of the tuning forks and ii) slight narrowing ($3-6$ %) of the structures in processing. The passband ripple and high loss are due to impedance mismatch at the input and output of the waveguide. Matched termination would require source and load impedances to equal the characteristic impedance Z_c given in table 1. The gentle slope of the measured responses in the lower passband edge can be due to the finite stiffness of the low-Q anchoring connects. For the higher passband frequencies, the consecutive resonators move mostly out of phase, which suppresses the anchor motions and the associated losses. The dip in figure 7 (b) is likely caused by unideal periodicity of the chain due to fabrication tolerances or by contamination.

Figure 8 shows the measured and simulated group delays for the resonator chains. As in the response of figure 7, the ripple is due to impedance mismatch. Simulation with matched source and load impedances removes the ripple and gives center-band group delays of 20 μs and 10 μs for chain 1 and chain 2, respectively, as indicated with a thick solid line in figure 8. This is in agreement with theoretical predictions when the fitted values for the spring coefficients in table 3 are used in (9).

5. Low-impedance design

As the above measurement results show, the analysis of section 2 can be used to design MEMS resonator-chain delay lines with record high time delays in a given physical size. However, to facilitate matched source and load termination for the MEMS delay line and to avoid using a differential readout (see figure 6), a much lower characteristic impedance, well below the pad (C_{pad}), feed-through (C_{thr}) and transducer (C_0) impedances, is needed than what was obtained above in table 3. As shown by (14) this can be achieved by enhancing the coupling, η, and by strenghtening the anchoring

Table 3. Parameter values for the tuning-fork resonators that give a better fit between simulations and measurements in figure 7 than the design values of table 1.

	fork 1	fork2	unit
k'	12.6	9.9	kN/m
K	8.5	3.3	
f_0	12	11	MHz
Δf	1.3	2.6	MHz
v_g^0	70	140	m/s
T_g^0	20	10	μs
Z_c	6	13	MΩ
B	42		μm
d	230		nm
Q	8000		

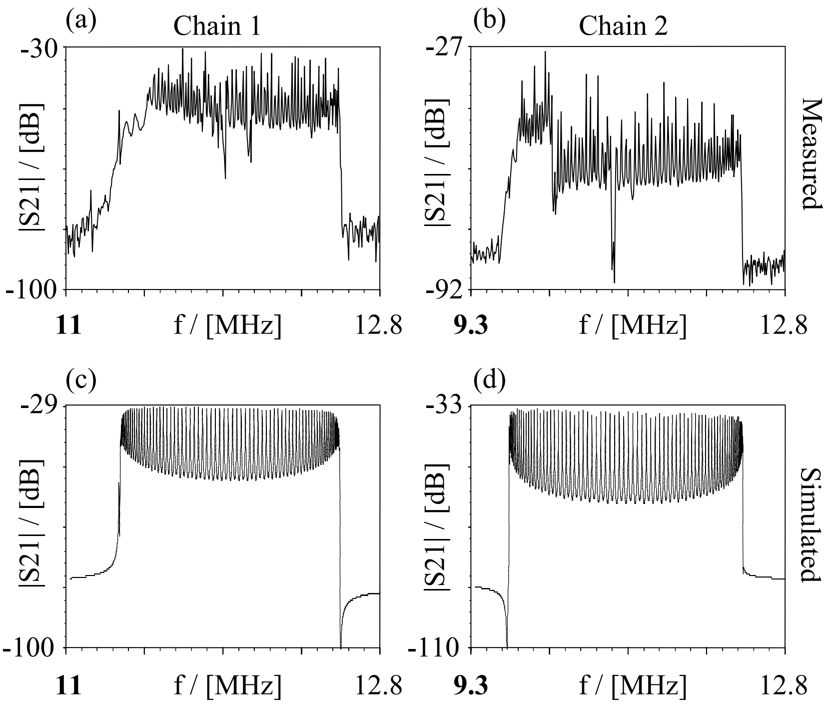

Figure 7. Measured ((a) and (b)) and simulated ((c) and (d)) $|S_{21}|$ for chain 1 ((a) and (c)) and chain 2 ((b) and (d)). The ripple is due to impedance mismatch at source and load.

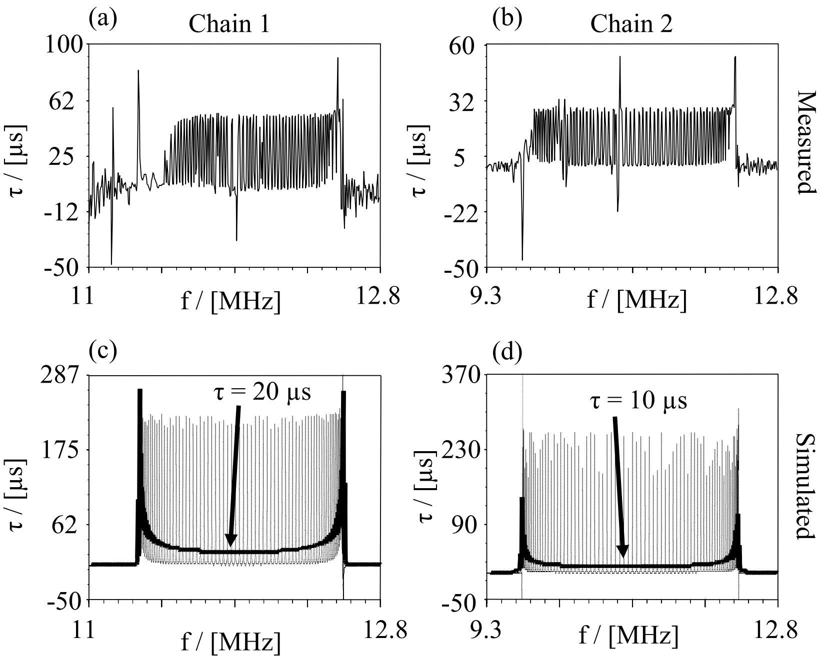

Figure 8. Measured and simulated group delay with ripple due to impedance mismatch as in figure 7. In simulation results ((c) and (d)) the thick solid curves show the group delay with impedance-matched source and load for the line.

spring, k', with respect to the coupling spring, k (larger K). Reducing the anchoring height, h_1, in figure 4 to 5 μm, doubling the beam separation ($w_f \rightarrow 20$ μm) and taking the narrowing of the structures in fabrication into account in design, a much higher spring-constant ratio of $K = 74$ is expected with $k' = 18$ kΩ and $M = 4.8$ ng. For good signal coupling, it is also important to design the first and last resonator in the chain to compensate for the electrical spring softening as well as for the stiffening of the first and last beams due to the capacitive coupling occuring over the transducer area as opposed to the point-force inter-resonator coupling along the chain. If, in addition, the transducer gap is reduced to $d = 100$ nm, a delay line with estimated characteristic impedance of $Z_c = 22$ kΩ (14), bandwidth of $\Delta f = 185$ kHz (7) and group velocity of $v_g^0 = 13$ m/s (9) can be obtained with a bias voltage of 30 V ($\eta = 11$ μFV/m).

Figure 9 shows the simulated response and group delay for a low-impedance chain of 80 resonators with reduced pad ($C_{pad} = 91$ fF $\Rightarrow Z_{pad} = 127$ kΩ) and feed-through capacitances ($C_{thr} = 8$ fF $\Rightarrow Z_{thr} = 1.3$ MΩ). The transducer capacitance is $C_0 = 37$ fF corresponding to $Z_0 = 308$ kΩ. Consequently, the characteristic impedance of the transmission line is much lower than Z_{pad}, Z_{thr} and Z_0 as required by good signal coupling. Figure 10 shows the corresponding simulation setup. To have a flat group delay at band center, resistive source and load termination to $R_L = 14$ kΩ was used that is somewhat lower than the estimated characteristic impedance of 22 kΩ. Higher pad and feed-through capacitances result in passband ripple and increased insertion loss if the characteristic impedance is not simultaneously further lowered.

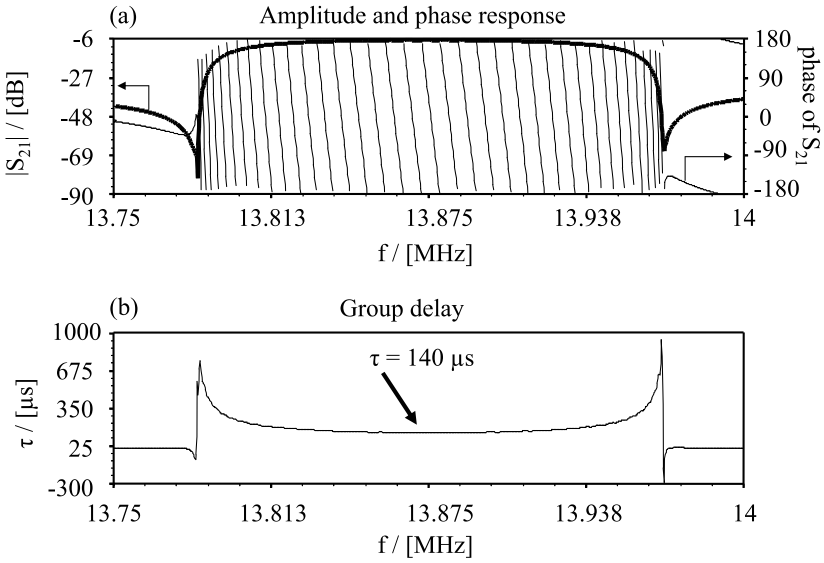

Figure 9. Simulated response (a) and group delay (b) for the low-impedance delay line with 14 kΩ source and load impedance. In (a) the thick line is for the amplitude and the thin line for the phase of S_{21}.

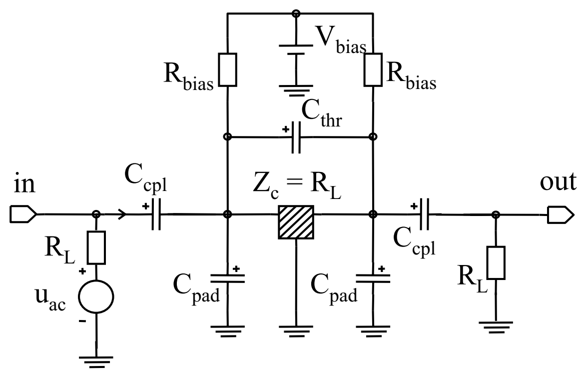

Figure 10. Simulation setup used to obtain the results of figure 9.

Figure 11 shows voltage amplitudes for a simulated transmission of a signal pulse through the delay line. The pulse duration is 115 μs to have the signal spectrum fit in the passband of the line. The signal frequency in the pulse is 13.875 MHz which is at the passband center. The rise time of the output voltage from 10 % to 90 % of the peak value in figure 11(b) is 15 μs.

6. Discussion and conclusions

A capacitively-coupled MEMS delay-line structure with record slow signal propagation was presented for HF frequencies enabling miniaturization of time-delay components. The properties of the delay line were theoretically analyzed and the theory was verified

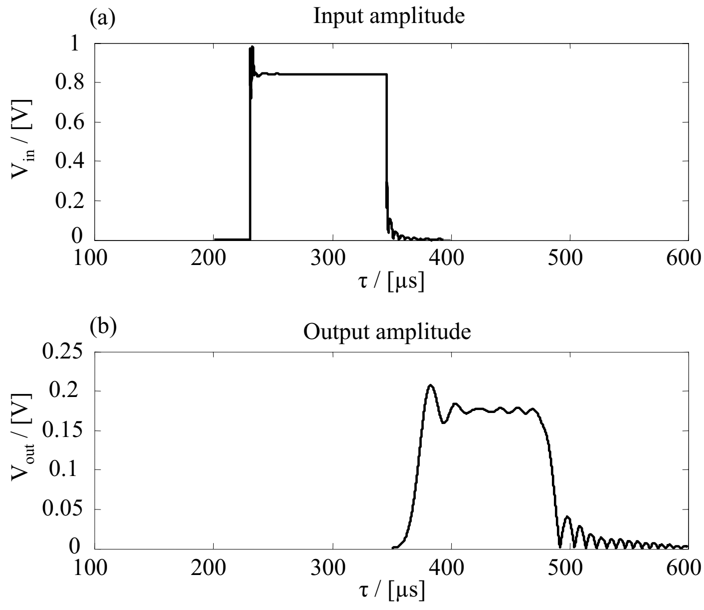

Figure 11. Simulated input (a) and output (b) voltage amplitudes for a pulse of width $\Delta T = 115$ μs transmitted through the delay line of figure 9 at the passband center.

in measurements with fabricated devices consisting of 80 series-connected MEMS resonators. The fabricated delay lines had too high characteristic impedances for practical applications but careful design can result in impedance levels of few kiloohms as shown in the paper. To reach higher frequencies, the resonator dimensions have to be scaled down which, however, weakens the capacitive coupling (increases the line impedance) unless the reduced transducer area is compensated by a smaller gap or a higher bias voltage. For clamped beams, the resonance frequency, f, depends on the width, w, and length, L, of the beam as $f \sim w/L^2$. Since the beam height, H, needs to be kept as high as possible for good coupling, fabrication tolerances easily limit the beam to be well thicker than a micrometer. Thus, for higher frequencies, a lower aspect ratio, L/w, of the beam is required which results in a lower quality factor, $Q \sim (L/w)^3$, due to clamping loss [24]. In addition to a group velocity that is much lower than for other acoustic delay lines (SAW or BAW), the MEMS line is characterized by a narrow-band response. This can be utilized in applications that would otherwise require a separate bandpass filter such as in wireless RF or ultrasound communication systems. For example, a low-power transponder terminal, communicating with on-off keying, is schematically shown in figure 12. Such transponders could be utilized, for example, in low-datarate sensor applications. Here, the reader sends an RF pulse to the sensor terminal in which the pulse is either retransmitted back to the reader (bit 1) or shunted to ground (bit 0).

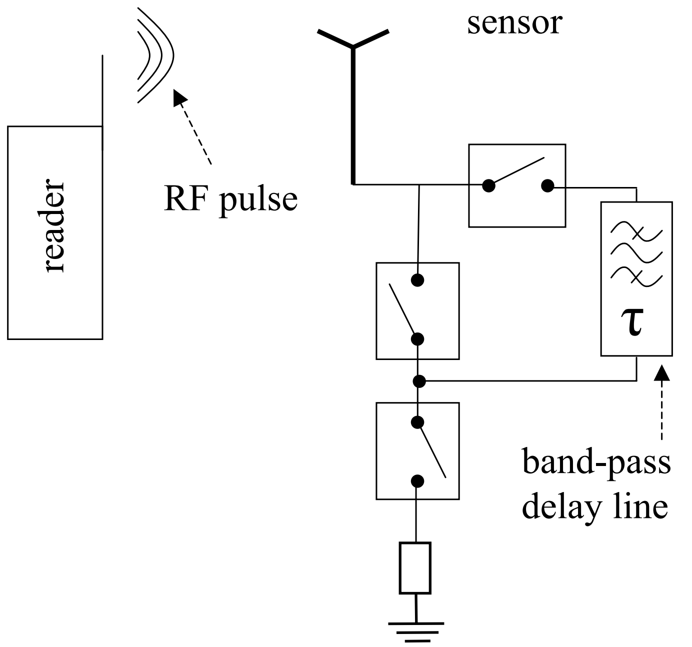

Figure 12. Schematic of a simple delay-line transponder for low-power low-datarate communication in sensor applications.

Acknowledgment

This work is supported by the Academy of Finland (grant 20542) and by Aplac® Solutions. The authors would like to thank Ville Kaajakari for discussions related to this paper.

References

[1] Weigel R, Morgan D P, Owens J M, Ballato A, Lakin K M, Hashimoto K and Ruppel C C W 2002 *IEEE Trans. Microwave Theory Tech.* **50** 738–749.
[2] Reindl L M, Pohl A, Scholl G and Weigel R 2001 *IEEE Sensors J.* **1** 69–78.
[3] Karilainen A, Finnberg T, Uelzen T, Dembowski K and Müller J 2004 *IEEE Trans. Ultrason., Ferroelect., Freq. Contr.* **51** 1464–1469.
[4] Narayanan R M, Zhou W, Wagner K H and Kim S 2004 *IEEE Geosci. Remote Sensing Lett.* **1** 166–170.
[5] Reindl L, Ruppel C C W, Berek S, Knauer U, Vossiek M, Heide P and Oréans L 2001 *IEEE Trans. Microwave Theory Tech.* **49** 787–794.
[6] Zari M C, Anderson C S and Caraway W D III 1995 *IEEE Trans. Microwave Theory Tech.* **43** 1889–1894.
[7] Salmon S K 1979 *IEEE Trans. Microwave Theory Tech.* **MTT-27** 1012–1018.
[8] Parker T E and Montress G K 1988 *IEEE Trans. Ultrason., Ferroelect., Freq. Contr.* **35** 342–364.
[9] Amorosi R I and Campbell C K 1985 *IEEE Trans. Sonics Ultrason.* **SU-32** 574–582.
[10] Ciplys D, Rimeika R, Sereika A, Gaska R, Shur M S, Yang J W and Khan M A 2001 *Electronics Letters* **37** 545–546.

[11] Kino G S, Ludvik S, Shaw H J, Shreve W R, White J M and Winslow D K 1973 *IEEE Trans. Microwave Theory Tech.* **MTT-21** 244–255.

[12] Berg N J, Lee J N, Casseday M W and Udelson B J 1979 *Applied Optics* **18** 2767–2774.

[13] Yin J H, Shen K X, Shui Y, Jiang Z L and He S P 1992 *Electronics Letters* **28** 172–174.

[14] Zhao S, Liu H and Tian Z 2004 In *Proc. IEEE Radio and Wireless Conference*, p 251–254.

[15] Kaajakari V, Mattila T, Oja A, Kiihamäki J and Seppä H 2004 *IEEE Electron Device Lett.* **25** 173–175.

[16] Nguyen C T C 1999 *IEEE Trans. Microwave Theory Tech.* **47** 1486–1503.

[17] Alastalo A T, Mattila T, Seppä H and Dekker J 2003 *Proc. 33rd European Microwave Conference* p 967–970.

[18] Lin L, Howe R T and Pisano A P 1998 *J. Microelectromech. Syst.* **7** 286–294.

[19] Ashcroft N W and Mermin N D 1976 *Solid State Physics* (Saunders College Publishing).

[20] Mattila T, Kiihamäki J, Lamminmäki T, Jaakkola O, Rantakari P, Oja A, Seppä H, Kattelus H and Tittonen I 1998 *Sensors and Actuators A* **101** 1–9.

[21] Ramo S, Whinnery J R and Duzer T V 1984 *Fields and Waves in Communication Electronics* (John Wiley & Sons) 2nd edition.

[22] Kiihamäki J, Kaajakari V, Luoto H, Kattelus H and Ylikoski M 2005 *Proc. The 13th International Conference on Solid State Sensors, Actuators and Microsystems, (Transducers'05)* p 1354–1357.

[23] Aplac RF Design Tool, APLAC Solutions Corp, www.aplac.com.

[24] Yasumura K Y, Stowe T D, Chow E M, Pfafman T, Kenny T W, Stipe B C and Rugar D 2000 *J. Microelectromech. Syst.* **9** 117–125.